31st Congress of the International Council of the Aeronautical Sciences

Belo Horizonte, Brazil; September 09-14, 2018

CONTROL OF A VERY FLEXIBLE WING WITH SIMULTANEOUS OPTIMIZATION OF THE GAIN MATRIX AND THE SPATIAL DISTRIBUTION OF THE SENSORS

Mauricio A. V. Morales* , Flávio J. Silvestre* , Antônio B. Guimarães Neto* , Gilles Tissot**
*Instituto Tecnológico de Aeronáutica, São José dos Campos, SP, 12228-900, Brazil , **Institut de Mathématiques de Toulouse, Université Paul Sabatier, 118 route de Narbonne - F-31062 Toulouse, France

Keywords: *very flexible wing, stabilization, optimal control*

Abstract

To stabilize a very flexible wing with a control system it is necessary to feedback wing measurements such as accelerations, deformations or displacements. In a previous work, displacement sensors were positioned at the wing tips and then the gain matrix of the feedback control was optimized. In this way, the performance of the control is restricted to the predetermined position of the sensors. Hence, in this paper we apply another methodology to simultaneously optimize the sensors positioning and the gain matrix. The results are compared in order to evaluate the benefits of this methodology in the considered problem.

1 Introduction

In general aviation, airframe structures are getting more efficient, decreasing weight and increasing flexibility. This trend demands further studies in non linear aeroelastic phenomena and their consequences in flying qualities, handling qualities, and automatic flight control. With this aim, University of Michigan developed the X-HALE aircraft, which has a replica being studied by the Instituto Tecnológico de Aeronáutica, shown in Fig. 1.

Fig. 1 The high flexibility of the X-HALE wing.

One of the challenges of a very flexible wing is the stabilization of the wing with control systems. In a previous work, this task was accomplished with displacement sensors at the wing tips [1]. In this paper we adopt another algorithm to optimize the sensor positioning together with the feedback control gains.

2 Model Description

The flexible aircraft model considered in this paper refers to the six-meter-span configuration (“6m”) of the X-HALE aircraft [2]. This configuration is known to be able to behave as a very flexible aircraft in certain longitudinal or lateral-directional maneuvers [3]. The physical-mathematical formulation upon which the numerical model is based was developed in Refs. [4] and [5], and a brief description is provided in section 2.1. Specific details about the aircraft model are contained in section 2.2.

2.1 Formulation

The equations of motion (EOMs) are derived using Lagrange's equation, and the flexible aircraft is treated as a three-dimensional body with discrete stiffness and inertia properties, using geometrically-linear beam finite elements. The elected set of $6+n$ generalized coordinates comprises: the components of the position vector $\mathbf{R}_{O,b}$ of the origin O of a body reference frame (BRF) expressed in the body axes, b; the Euler angles providing the orientation of the BRF with respect to the flat-Earth inertial reference frame (IRF): ψ, θ, and ϕ; and n elastic degrees of freedom (DOFs) of the aircraft structure, constituting the displacement vector $\mathbf{u}_G = \begin{Bmatrix} u_1 & u_2 & \cdots & u_n \end{Bmatrix}^T$. The resulting EOMs read:

$$\begin{aligned} &m\dot{\mathbf{V}}_b + m\widetilde{\boldsymbol{\omega}}_b\mathbf{V}_b - m\widetilde{\mathbf{s}_{CG,b}}\dot{\boldsymbol{\omega}}_b - m\widetilde{\boldsymbol{\omega}}_b\widetilde{\mathbf{s}_{CG,b}}\boldsymbol{\omega}_b \\ &\quad + m\widetilde{\dot{\boldsymbol{\omega}}}_b\mathbf{D}_{CG,b}\mathbf{u}_G + 2m\widetilde{\boldsymbol{\omega}}_b\mathbf{D}_{CG,b}\dot{\mathbf{u}}_G \qquad (1) \\ &+ m\widetilde{\boldsymbol{\omega}}_b\widetilde{\boldsymbol{\omega}}_b\mathbf{D}_{CG,b}\mathbf{u}_G + m\mathbf{D}_{CG,b}\ddot{\mathbf{u}}_G = m\mathbf{g}_b + \mathbf{F}_b + \Delta\mathbf{F}_b, \end{aligned}$$

$$\begin{aligned} &\mathbf{J}_O\dot{\boldsymbol{\omega}}_b + \widetilde{\boldsymbol{\omega}}_b\mathbf{J}_O\boldsymbol{\omega}_b + m\widetilde{\mathbf{s}_{CG,b}}\left(\dot{\mathbf{V}}_b + \widetilde{\boldsymbol{\omega}}_b\mathbf{V}_b\right) \\ &\quad + m\widetilde{\mathbf{D}_{CG,b}\mathbf{u}_G}\left(\dot{\mathbf{V}}_b + \widetilde{\boldsymbol{\omega}}_b\mathbf{V}_b\right) \\ &\quad + \Delta\mathbf{J}'_O\dot{\boldsymbol{\omega}}_b + \widetilde{\boldsymbol{\omega}}_b\Delta\mathbf{J}'_O\boldsymbol{\omega}_b + \Delta\dot{\mathbf{J}}'_O\boldsymbol{\omega}_b \qquad (2) \\ &\quad + \dot{\mathbf{M}}_{\boldsymbol{\omega}G}\dot{\mathbf{u}}_G + \mathbf{M}_{\boldsymbol{\omega}G}\ddot{\mathbf{u}}_G + \widetilde{\boldsymbol{\omega}}_b\mathbf{M}_{\boldsymbol{\omega}G}\dot{\mathbf{u}}_G \\ &= m\widetilde{\mathbf{s}_{CG,b}}\mathbf{g}_b + m\widetilde{\mathbf{D}_{CG,b}\mathbf{u}_G}\mathbf{g}_b + \mathbf{M}_{O,b} + \Delta\mathbf{M}_{O,b}, \end{aligned}$$

$$\begin{aligned} &\mathbf{M}_{GG}\ddot{\mathbf{u}}_G + \mathbf{B}_{GG}\dot{\mathbf{u}}_G + \mathbf{K}_{GG}\mathbf{u}_G \\ &+ m\mathbf{D}_{CG,b}{}^T\left(\dot{\mathbf{V}}_b + \widetilde{\boldsymbol{\omega}}_b\mathbf{V}_b\right) + \mathbf{M}_{\boldsymbol{\omega}G}{}^T\dot{\boldsymbol{\omega}}_b \\ &+ 2\dot{\mathbf{M}}^T_{\boldsymbol{\omega}G}\boldsymbol{\omega}_b - \frac{1}{2}\sum_{g=1}^{n}\mathbf{e}_{n,g}\boldsymbol{\omega}_b{}^T\frac{\partial\Delta\mathbf{J}_O}{\partial u_g}\boldsymbol{\omega}_b \qquad (3) \\ &= m\mathbf{D}_{CG,b}{}^T\mathbf{g}_b + \mathbf{Q}_G. \end{aligned}$$

In Eqs. (1)-(3), $\boldsymbol{\omega}_b = \begin{Bmatrix} p & q & r \end{Bmatrix}^T$ is the angular velocity vector of the BRF with respect to the IRF; $\mathbf{V}_b = \begin{Bmatrix} u & v & w \end{Bmatrix}^T$ is the velocity vector of the BRF origin O with respect to the IRF; the skew-symmetric operator, $\widetilde{(\bullet)}$ or skew $(\bullet)$, denotes the matrix-form of the vector cross product; m is the aircraft total mass; $\mathbf{s}_{CG,b}$ refers to the CG position vector in the undeformed (unstrained) condition; $\mathbf{d}_{CG,b} = \mathbf{D}_{CG,b}\mathbf{u}_G$ stands for the change in $\mathbf{s}_{CG,b}$ due to structural deformation; $\mathbf{J}_O$ is the inertia matrix about O; $\Delta\mathbf{J}'_O$ is the change in the inertia matrix due to structural deformation; $\mathbf{M}_{GG}$, $\mathbf{B}_{GG}$, and $\mathbf{K}_{GG}$ are the finite-element method (FEM) model mass, damping and stiffness matrices, respectively; $\mathbf{F}_b$ and $\mathbf{M}_{O,b}$ are the net force and moment vectors, respectively, associated with the rigid airframe; $\Delta\mathbf{F}_b$ and $\Delta\mathbf{M}_{O,b}$ are the net incremental force and moment vectors, respectively, due to elastic motion; $\mathbf{g}_b$ is the gravity vector expressed in the BRF; $\mathbf{Q}_G$ is the column matrix of generalized aerodynamic and propulsive forces; at last, $\mathbf{M}_{\boldsymbol{\omega}G}$ is the inertia coupling matrix between the rotational rigid-body and the elastic DOFs. The total number of elastic DOFs is n. The notation $\mathbf{e}_{N,i}$ represents a column matrix equal to the ith column of the identity matrix of order N, $\mathbf{I}_N$. All time derivatives are taken in the BRF.

The FEM stiffness matrix, $\mathbf{K}_{GG}$, refers to an unrestrained 3D structure and hence it is a positive semi-definite matrix, with six linearly-independent rigid-body motions allowed. This rigid-body freedom of the FEM model is not desired, since the coordinates of the origin O and the Euler angles were already considered to be the rigid-body DOFs of the flexible aircraft. The six constraints needed to eliminate the rigid-body motion from the elastic DOFs were proposed in the the so-called dually-constrained axes (DCA) [5], and are considered in this paper as well.

In this paper, the aerodynamic loads acting on the flexible aircraft are obtained with the vortex- [6] (VLM) and the doublet-lattice [7] (DLM) methods. The XFOIL program [8] is coupled with the VLM to yield the rigid-body aerodynamic databank, which takes into account nonlinear Reynolds number and angle of attack effects, including stall. The incremental aerodynamic loads that arise due to the airframe flexibility are first calculated in the frequency domain with the DLM and are then converted to the time domains using rational function approximations [9]. The incremental loads are corrected with multiplying factors that vary with the Reynolds number and the angle of attack [10]. At last, induced drag disturbances are also taken into account, based

on the methodology proposed in Ref. [11] and adapted in Ref. [4].

2.2 The X-HALE model

The six-meter-span configuration of the X-HALE comprises six wing panels of one-meter span and twenty-centimeter chord each. The wing tip panels have positive dihedral angle of 10 degrees. The whole wing is built with an incidence of 5 degrees. The wing airfoil is a reflexed EMX-07 [2]. The aircraft also has five pods at the connections between wing sections. The aircraft engines, landing gears, electronics and some of the sensors are installed at the pods.

Four boom-mounted, all-moving horizontal stabilizers are installed at the connections between the wing panels, except at the central connection, where a fifth boom-mounted tail is installed without variable incidence but with a flip-up capability, allowing it to be positioned either as a horizontal tail or as a vertical tail. However, only the configuration with a horizontal central tail ('XH6h') is analyzed in this paper. All tails have NACA0012 airfoil as cross sections.

The aerodynamic model is based on the VLM [6] and the DLM [7]. Both methods share the same mesh, built considering the guidelines proposed in Ref. [12], which result in a model with the significant amount of 3327 boxes. The aerodynamic mesh is shown in Fig. 2.

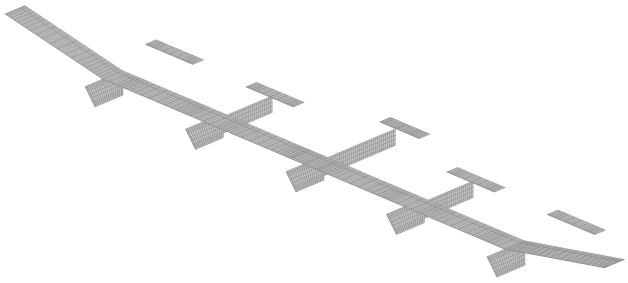

Fig. 2 Isometric view of the VLM mesh for the X-HALE XH6h configuration.

The XH6h configuration has six control surfaces with variable deflections: left and right ailerons installed at the wing tip, dihedral sections, with deflections $\delta_{l_{ail}}$ and $\delta_{r_{ail}}$, respectively; and two outer and two inner left and right boom-mounted elevons, with deflections $\delta_{lo_{elev}}$, $\delta_{ro_{elev}}$, $\delta_{li_{elev}}$ and $\delta_{ri_{elev}}$. The aircraft also has five pod-mounted tractor electric motors, with throttle settings represented by $\delta_{lo_{thr}}$, $\delta_{li_{thr}}$, $\delta_{c_{thr}}$, $\delta_{ri_{thr}}$, and $\delta_{ro_{thr}}$, for the left outer, left inner, central, right inner and right outer motors, respectively. The control surfaces and motors are schematically represented in Fig. 3.

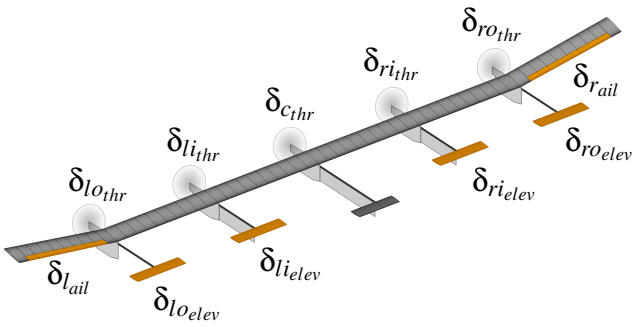

Fig. 3 The X-HALE XH6h control surfaces and electric motors.

The structural-dynamic model consists of geometrically-linear beam finite elements for the wing and booms and rigid bars for the tails. Ten beam elements per wing section are used. Modal superposition is used to reduce the size of the problem, yielding a drastic reduction of the number of degrees of freedom implicit in Eq. (3), from the original amount of 528 independent FEM DOFs to 14 modes of vibration. Of the set of fourteen modes of vibration, the first three wing bending modes (aircraft first, third and fifth modes) are the most relevant ones for the present application, and are shown in Fig. 4.

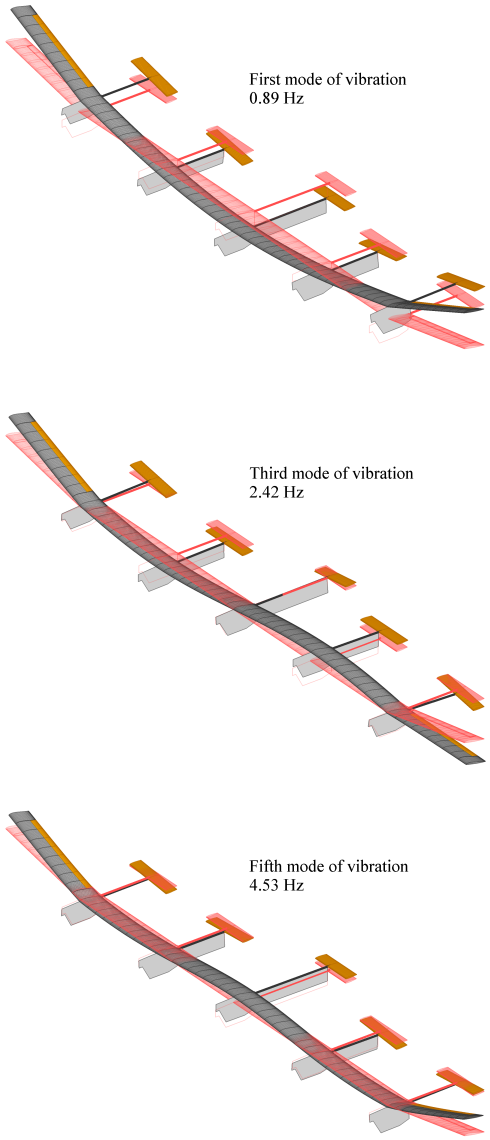

Fig. 4 First three wing bending modes of vibration of the XH6h configuration.

2.3 Linear model for control design

The nonlinear simulation model is trimmed in level flight condition at an altitude of 650 meters in the ISA, and the design flight speed of 14 m/s is considered in the studies developed in this paper. The nonlinear equations of motion are then linearized around the calculated equilibrium condition, yielding a classical linearized model as follows:

$$\begin{aligned} \dot{\mathbf{x}} &= A\mathbf{x} + B\mathbf{u}, \\ \mathbf{y} &= C\mathbf{x} + D\mathbf{u}, \end{aligned} \tag{4}$$

where the vector of disturbances of the state variables around the equilibrium conditions is given by $\mathbf{x} = \left\{ \mathbf{x}_{rigid}{}^T \quad \mathbf{x}_{flex}{}^T \right\}^T$, with:

$$\begin{aligned} \mathbf{x}_{rigid} = \big\{ &\Delta V \quad \Delta\alpha \quad \Delta q \quad \Delta\theta \\ &\Delta\beta \quad \Delta\phi \quad \Delta p \quad \Delta r \big\}^T, \end{aligned} \tag{5}$$

$$\begin{aligned} \mathbf{x}_{flex} = \big\{ &\Delta\eta_1 \quad \cdots \quad \Delta\eta_{14} \\ &\dot{\eta}_1 \quad \cdots \quad \dot{\eta}_{14} \\ &\eta_{1,lag(1)} \quad \cdots \quad \eta_{14,lag(7)} \big\}^T, \end{aligned} \tag{6}$$

for the 14-mode dynamics and the 14-mode, 7th-order aerodynamic lag dynamics of the flexible aircraft; $\mathbf{u}$ is the vector of disturbances of the control variables:

$$\begin{aligned} \mathbf{u} = \big\{ &\Delta\delta_{l_{ail}} \quad \Delta\delta_{lo_{elev}} \quad \Delta\delta_{li_{elev}} \quad \Delta\delta_{ri_{elev}} \quad \Delta\delta_{ro_{elev}} \\ &\Delta\delta_{lo_{thr}} \quad \Delta\delta_{li_{thr}} \quad \Delta\delta_{c_{thr}} \quad \Delta\delta_{ri_{thr}} \quad \Delta\delta_{ro_{thr}} \big\}^T, \end{aligned} \tag{7}$$

$\mathbf{y}$ is a vector containing a set of selected output variables to be monitored; and A, B, C and D are the matrices resulting from the numerical linearization procedure.

Models with less than 14 modes of vibration and without aerodynamic lag states can be obtained applying the residualization technique developed in Ref. [4], in which the states with neglected dynamics become linear algebraic functions of the remaining states. In this context, models without aerodynamic lag dynamics and models with only the first two or the first three wing bending modes, in addition to the rigid-body states, were obtained and are used in the following sections.

3 Control Problem Statement

In the following applications, the output $\mathbf{y}$ does not depent directy on the control variables, therefore the matrix D is null, and the Eq. 4 is simplyfied to:

$$\dot{\mathbf{x}} = A\mathbf{x} + B\mathbf{u} \tag{8}$$

$$\mathbf{y} = C\mathbf{x} \tag{9}$$

where $\mathbf{x} \in \mathbb{R}^n$ is the state, $\mathbf{u} \in \mathbb{R}^c$ is the control input, and $\mathbf{y} \in \mathbb{R}^m$ is the output.

The control problem of interest is to drive the system back to the operating point ($\mathbf{x} = \mathbf{0}$) using an output feedback control:

$$\mathbf{u} = -K\mathbf{y}, \tag{10}$$

with the gain matrix K that minimizes the following quadratic performance index:

$$\mathcal{J} = \frac{1}{2}\int_0^\infty \left(\mathbf{x}^T Q\mathbf{x} + \mathbf{u}^T R\mathbf{u}\right)\mathrm{d}t, \tag{11}$$

where Q and R are given symmetric and positive semi-definite weighting matrices.

Stevens et al. [13] show that this optimal control problem can be transformed in the problem of finding the K matrix that minimizes:

$$\mathcal{J} = \frac{1}{2}\mathrm{tr}(PX), \tag{12}$$

where $X = \mathbf{x}(0)\mathbf{x}(0)^T$, $\mathbf{x}(0)$ is a perturbed initial condition, P is the solution of:

$$A_c^T P + PA_c + C^T K^T BKC + Q = 0, \tag{13}$$

and $A_c = A - BKC$ is the state matrix of the closed loop system, obtained by replacing the control law (Eq. 10) and the output equation (Eq. 9) in the state equation (Eq. 8).

Then, to solve this problem numerically, a minimization algorithm must be applied to a function that outputs $\mathcal{J}$ (Eq. 12) for each inputed K matrix and the corresponding P matrix (Eq. 13). The gradient of this minimization is given by:

$$\frac{\partial \mathcal{J}}{\partial K} = RKCSC^T - B^T PSC^T \tag{14}$$

where S is the solution of:

$$A_c S + SA_c^T + \mathbf{x}(0)\mathbf{x}(0)^T = 0 \tag{15}$$

González *et* al. [1] applied this methodology to find the optimal gain to stabilize the X-HALE rigid body modes and the wing shape by feedbacking an output composed by some rigid body variables and the displacements at the wing tips. In this study, another issue is posed: what would be the optimal displacement sensor positioning? One approach would be to calculate the matrix gain for a given sensor positioning and then repeat this procedure for many different positionings and verify the lowest performance index. To avoid a parametric optimization, a new methodology was applied, detailed in the next section.

4 Applied New Methodology For Optimal Sensor Positioning

In a paper under consideration for publication in Journal of Fluid Mechanics, Silvestre and Tissot [14] developed a methodology to optimize simultaneously the gains of the feedback control and the positions of the sensors in a flow control problem. We now apply this methodology to the control problem described in the previous section.

Let $x_s(j)$ be the position of the j-th sensor along the wing span, and $\mathbf{x}_s$ the array containing the positions of all sensors. Then, output matrix is now denoted $C(\mathbf{x}_s)$ For this, the Lagrangian of the system $\mathcal{L}$ is defined as:

$$\mathcal{L}(\mathbf{x}, \mathbf{x}_s, K, \lambda) = \mathcal{J}(\mathbf{x}, \mathbf{x}_s, K) - \int_0^T \left(\lambda, \frac{\mathrm{d}\mathbf{x}}{\mathrm{d}t} - A_c(\mathbf{x}_s)\mathbf{x}\right)\mathrm{d}t, \tag{16}$$

where λ is the vector of Lagrange multipliers and $A_c(\mathbf{x}_s) = A - BKC(\mathbf{x}_s)$ is the state matrix of the closed loop system. Proceeding this way, it can be shown [14] that the gradient of $\mathcal{J}$ with respect to each element $x_{s(j)}$ of the vector $\mathbf{x}_s$ is:

$$\frac{\partial \mathcal{J}}{\partial x_{s(j)}} = \mathrm{tr}\left(S\left(C^T K^T R - P^T B\right)K\frac{\partial C}{\partial x_{s(j)}}\right), \tag{17}$$

and that the resulting system to be solved is given by Eqs. 13, 14, 15, and 17.

5 Feedback Structure

The output feedback law (Eq. 10) permits to feed back all the output variables in each of the control variables. However, this is not necessary and neither practical. To give the controller more structure, some of the gains in the gain matrix K are zeroed based on the flight physics [13] as follows.

To augment the stability of an aircraft with conventional control surfaces, the roll rate p is typically fed back in the aileron control u_{ail}, the pitch rate q in the elevon control u_{elev}, and the yaw rate r in the rudder u_{rud}:

$$u_{ail} = -k_p p \tag{18}$$
$$u_{elev} = -k_q q \tag{19}$$
$$u_{rud} = -k_r r \tag{20}$$

This is based on the physical fact that the aileron, elevator and rudder deflections produce rolling, pitching and yawing moments respectively. The X-HALE has conventional ailerons, then aileron control u_{ail} is distributed antisymmetrically in the aileron deflections $\Delta\delta_{l_{ail}}$ and $\Delta\delta_{r_{ail}}$:

$$\Delta\delta_{l_{ail}} = -u_{ail} \tag{21}$$
$$\Delta\delta_{r_{ail}} = +u_{ail} \tag{22}$$

To reproduce the elevator deflection in the X-HALE, the inner elevons $\Delta\delta_{li_{elev}}$ and $\Delta\delta_{ri_{elev}}$ were deflected symmetrically:

$$\Delta\delta_{li_{elev}} = u_{elev} \tag{23}$$
$$\Delta\delta_{ri_{elev}} = u_{elev} \tag{24}$$

And to reproduce the rudder deflection, the outer motors $\Delta\delta_{lo_{thr}}$ and $\Delta\delta_{ro_{thr}}$ were commanded antisymmetrically:

$$\Delta\delta_{lo_{thr}} = -u_{rud} \tag{25}$$
$$\Delta\delta_{ro_{thr}} = +u_{rud} \tag{26}$$

To control the wing shape, vertical translational structural displacements t_z were fed back in the outer elevons. For example, in the case of two measurements in the left half-wing $\{t_{zl_1}, t_{zl_2}\}$ and two measurements in the right half-wing $\{t_{zr_1}, t_{zr_2}\}$ they were all fed back in both left and right outer elevons $\Delta\delta_{lo_{elev}}$ and $\Delta\delta_{ro_{elev}}$:

$$\begin{aligned}\Delta\delta_{lo_{elev}} = u_{lo_{elev}} = &-k_{lo_{elev,l_1}} t_{zl_1} - k_{lo_{elev,l_2}} t_{zl_2} \\ &- k_{lo_{elev,r_1}} t_{zr_1} - k_{lo_{elev,r_2}} t_{zr_2}\end{aligned} \tag{27}$$

$$\begin{aligned}\Delta\delta_{ro_{elev}} = ro_{elev} = &-k_{ro_{elev,l_1}} t_{zl_1} - k_{ro_{elev,l_2}} t_{zl_2} \\ &- k_{ro_{elev,r_1}} t_{zr_1} - k_{ro_{elev,r_2}} t_{zr_2}\end{aligned} \tag{28}$$

Neither the central motor ($\Delta\delta_{c_{thr}}$) nor the inner motors ($\Delta\delta_{li_{thr}}$, $\Delta\delta_{li_{thr}}$) were not considered in this control struture because they were not necessary to achieve the desired regulation.

6 Results For Optimal Sensor Positioning

As only vertical translational structural displacements were considered in the feedback structure, the adopted model included only the first three wing bending modes of vibration, corresponding to the η_1, η_3, and η_5 degrees of freedom.

To weight each state variable individually in the performance index $\mathcal{J}$, the chosen state weighting matrix Q was diagonal. This way, the i-th element q_i of the diagonal weights the i-th state variable x_i. The second and the third bending modes are less pronounced than the first bending mode, therefore they had to be more weighted than the others. The assumed values are in Tab. 1.

Table 1 Chosen diagonal elements of the state weighting matrix Q

$q_i = 0.025$, for $i \neq \{\eta_3, \eta_5, \dot{\eta}_3 \dot{\eta}_5\}$	
$q_{\eta_3} = 9q_i$	$q_{\dot{\eta}_3} = 9q_i$
$q_{\eta_5} = 900q_i$	$q_{\dot{\eta}_5} = 900q_i$

The control weighting matrix R was also chosen diagonal, to penalize the use of each control variable individually. Different values were adopted for each element based on their admitted values, as shown in Tab. 2

Table 2 Chosen diagonal elements of the control weighting matrix R

$r_{u_{ail}} = 0.5/(1^2)$	$r_{lo_{elev}} = 0.5/(0.2^2)$
$r_{u_{elev}} = 0.5/(0.5^2)$	$r_{ro_{elev}} = 0.5/(0.2^2)$
$r_{u_{rud}} = 0.5/(0.1^2)$	

The positions of the sensors were constrained to be mirrored with respect to the central pod. For instance, the distance of the first left sensor that measures t_{zl_1} is the same of the first right sensor that measures t_{zr_1} with respect to the central pod. Then, in the following results the sensor positions

are shown only for one half-wing. The central pod corresponds to 0 m and the wing tip corresponds to 2.98 m.

Two types of optimizations were studied in this paper, first with only 1 sensor in each half-wing, and then with 2 sensors.

6.1 Optimizations with 1 sensor

Since the numerical optimization algorithm is not global, it was initialized with 5 different sensor positions. In this way, the performance indexes could be compared to eliminate a suboptimal result. Table 3 shows, for each optimization case, the initial position, the correponding optimal final position and the resulting performance index.

Table 3 Optimizations with 1 sensor in each half-wing, stating from different initial positions

optimization ID	initial position	final position	$\mathcal{J}$
1s1	1.50	2.98	42.1069
1s2	1.87	2.98	42.1069
1s3	2.24	2.98	42.1069
1s4	2.61	2.98	42.1069
1s5	2.98	2.98	42.1069

All of them converged to the same final position at the wing tip, confirming the choice made by [1]. The reason for this may be the first bending mode, in which the wing tip presents the maximum displacement.

In Fig.5 the optimal sensor positioning can be seen evolving along the iterations, starting from different initial positions (0%) and arriving at the wing tip (100%). It also can be seen in this figure that the algorithm is able to explore great part of the domain before converging, which is desirable to ensure globality to the results.

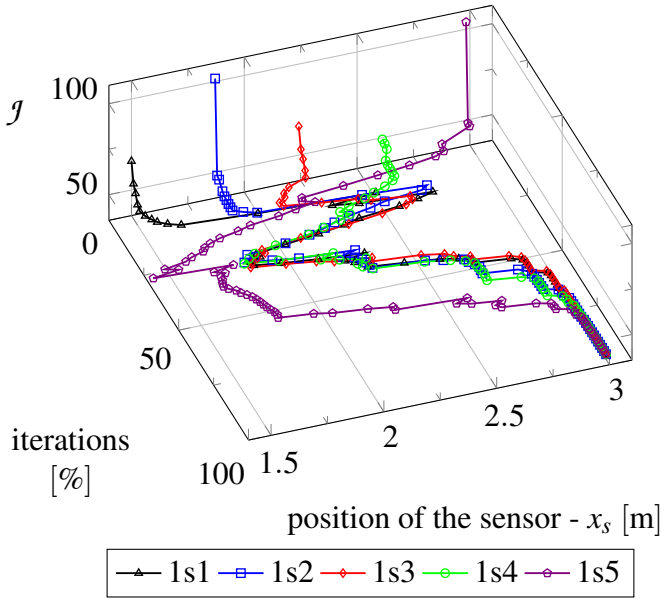

Fig. 5 Optimizations with 1 sensor in each half-wing.

Figure 6 highlights the lasts iterations of the positions and corresponding performance indexes.

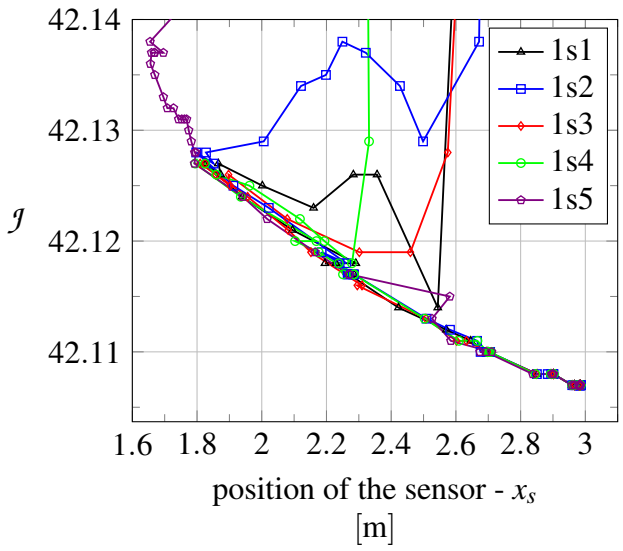

Fig. 6 Last iterations of the optimizations with 1 sensor in each half-wing.

For the sake of completeness, the optimal gains are shown in Tab. 4, which resulted to be the same for the 5 optimizations.

Table 4 Optimal gains and sensor position for 1 sensor in each half-wing

$k_q = -0.0262$	$k_{lo_{elev,r}} = 1.9016$
$k_p = -0.3862$	$k_{ro_{elev,l}} = 1.8688$
$k_r = -0.0177$	$k_{ro_{elev,r}} = 1.8393$
$k_{lo_{elev,l}} = 1.8588$	$x_s = 2.98$

6.2 Optimizations with 2 sensors

In the same manner of the optimizations with 1 sensor, 5 different optimizations were made when considering 2 sensors for each half-wing. Table 5 shows, for each optimization case, the initial position, the correponding optimal final position and the resulting performance index.

Table 5 Optimizations with 2 sensors in each half-wing, stating from different initial positions

optimization ID	initial positions	final positions	$\mathcal{J}$
2s1	{1.50,2.98}	{2.00,2.98}	42.1062
2s2	{1.69,2.81}	{2.00,2.98}	42.1062
2s3	{1.88,2.64}	{2.00,2.98}	42.1062
2s4	{2.06,2.47}	{2.98,2.00}	42.1062
2s5	{2.25,2.30}	{2.00,2.98}	42.1062

All the optimizatins converged to one sensor being positioned at 2 m and the other at the wing tip. The position at 2 m is not intuitive because in the first three bending modes it does not stand out in terms of displacements (see Fig. 4), but it is worth remembering that the displacements along the wing result from the composition of the different modes.

In Fig.7 the optimal sensors positioning can be seen evolving along the iterations, starting from different initial positions (0%) and one arriving at 2 m and the other at the wing tip (100%). As in the cases with only one sensor, it also can be seen in this figure that the algorithm is able to explore great part of the domain before converging, which is desirable to increase globality to the results.

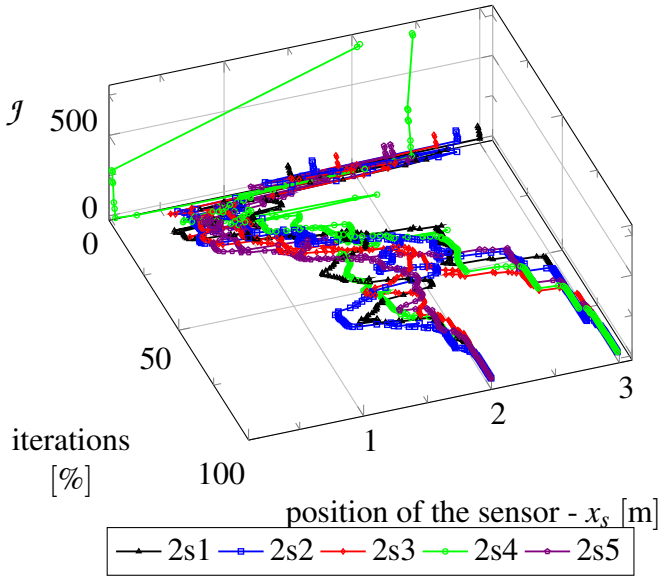

Fig. 7 Optimizations with 2 sensors in each half-wing.

The lasts iterations of the positions and corresponding performance indexes are shown in Fig 8.

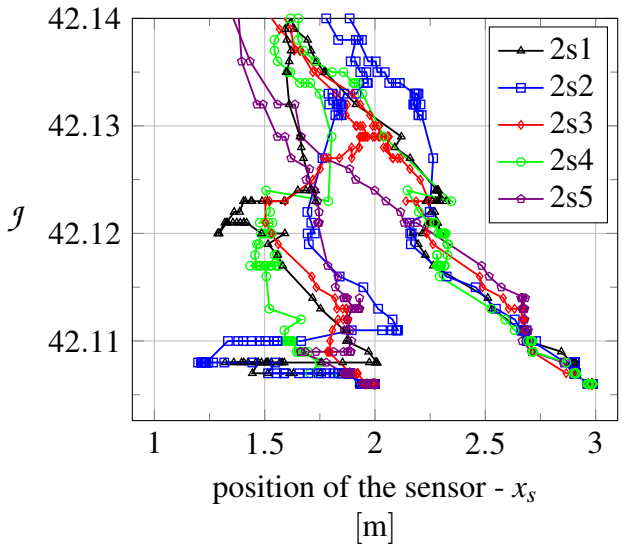

Fig. 8 Last iterations of the optimizations with 2 sensors in each half-wing.

And the optimal gains are shown in Tab. 6, which also resulted to be the same for the 5 optimizations. Actually, in the optimization "2s4" some of the gains interchanged because in this case the sensors changed positions, which can be seen in Tab. 5.

Table 6 Optimal gains and sensors positions for 2 sensors in each half-wing

$k_q = -0.0262$	$k_{ro_{elev,l1}} = -1.0714$
$k_p = -0.3860$	$k_{ro_{elev,l2}} = 2.3948$
$k_r = -0.0177$	$k_{ro_{elev,r1}} = -0.9477$
$k_{lo_{elev,l_1}} = -0.6465$	$k_{ro_{elev,r2}} = 2.3136$
$k_{lo_{elev,l_2}} = 2.2084$	$x_{s_1} = 2.00$
$k_{lo_{elev,r_1}} = -1.3985$	$x_{s_2} = 2.98$
$k_{lo_{elev,r_2}} = 2.5649$	

Finally, simulations were carried out to compare the open-loop and the closed-loop responses, with 1 and 2 sensors. Figure 9 shows the responses of the wing tip displacements when the aircraft was initially perturbed in it's flight speed.

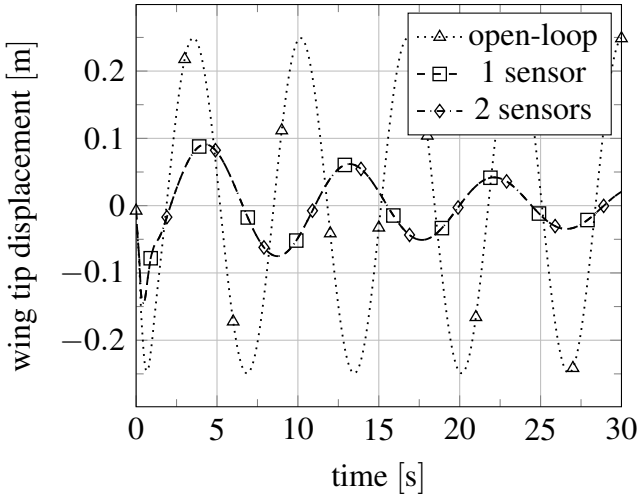

Fig. 9 Responses of the wing tip displacements under an initially perturbed flight speed.

The closed loop responses are clearly more damped than the open loop one. However, between 1 and 2 sensors there is little difference. This was predictable since the obtained optimized performance indexes were too similar (see Tabs. 3 and 5).

7 Conclusions

In this paper, vertical translational displacements at the wing of a flexible aircraft were feed back to stabilize the wing shape. For the first time, a new methodology was applied to simultaneously optimize the spatial distribution of the sensors and the feeback gains. When only one sensor was considered, the optimal position obtained was the wing tip. And when two sensors were considered, they converged to different positions, one at the wing tip and other at $2/3$ of the wing. Adding the second sensor did not reduce significantly the performance index, which was confirmed comparing the responses over time. Maybe with other weighting matrices the results between one and two sensors could be different, this must be verified in further studies.

Only displacements along the elastic axis were considered in this paper because the goal was to control the bending modes. In future work, displacements outside the elastic line should be included to the control also torsion modes.

Contact Author Email Address

morales@ita.br

Acknowledgement

This work has been funded by FINEP and EMBRAER under the research project Advanced Studies in Flight Physics, contract number 01.14.0185.00.

Copyright Statement

References

[1] P. J. González, A. B. Guimarães Neto, G. C. Barbosa, R. M. Bertolin, F. J. Silvestre, and

C. E. S. Cesnik, "X-hale autopilot with stability augmentation and shape control based on loop separation," (Como, Italy), IFASD - International Forum on Aeroelasticity and Structural Dynamics, 25–28 June 2017.

[2] C. E. S. Cesnik, P. J. Senatore, W. Su, E. M. Atkins, and C. M. Shearer, "X-hale: A very flexible unmanned aerial vehicle for nonlinear aeroelastic tests," *AIAA Journal*, vol. 50, no. 12, pp. 2820–2833, 2012.

[3] A. B. Guimarães Neto, F. L. Cardoso-Ribeiro, and F. J. Silvestre, "Applicability of geometrically-linear structural-dynamic models for the flight dynamics of arbitrarily-flexible aircraft," (Belo Horizonte, Brazil), ICAS - 31st Congress of the International Council of the Aeronautical Sciences, 9-14 September 2018.

[4] A. B. Guimarães Neto, *Flight dynamics of flexible aircraft using general body axes: a theoretical and computational study*. PhD thesis, Instituto Tecnológico de Aeronáutica, 2014.

[5] A. B. Guimarães Neto, R. G. A. Silva, P. Paglione, and F. J. Silvestre, "Formulation of the flight dynamics of flexible aircraft using general body axes," *AIAA Journal*, vol. 54, no. 11, pp. 3516–3534, 2016.

[6] S. G. Hedman, "Vortex lattice method for calculation of quasi steady state loadings on thin elastic wings," Rpt. 105, Aeronaut. Res. Inst. of Sweden, Stockholm, Sweden, 1965.

[7] E. Albano and W. P. Rodden, "A doublet-lattice method for calculating lift distributions on oscillating surfaces in subsonic flows," *AIAA Journal*, vol. 7, no. 2, pp. 279–285, 1969.

[8] M. Drela, "XFOIL: An analysis and design system for low reynolds number airfoils," in *Low Reynolds Number Aerodynamics* (T. Mueller, ed.), vol. 54 of *Lecture Notes in Engineering*, pp. 1–12, Springer Berlin Heidelberg, 1989.

[9] W. Eversman and A. Tewari, "Consistent rational function approximation for unsteady aerodynamics," *Journal of Aircraft*, vol. 29, no. 9, pp. 545–552, 1991.

[10] J. P. Giesing, T. P. Kálmán, and W. P. Rodden, "Correction factor techniques for improving aerodynamic prediction methods," nasa-cr-144967, McDonnell Douglas Corporation, 1976.

[11] T. P. Kálmán, J. P. Giesing, and W. P. Rodden, "Spanwise distribution of induced drag in subsonic flow by the vortex lattice method," *Journal of Aircraft*, vol. 7, no. 6, pp. 574–576, 1970.

[12] W. P. Rodden, P. F. Taylor, S. C. McIntosh, and M. L. Baker, "Further convergence studies of the enhanced doublet-lattice method," *Journal of Aircraft*, vol. 36, no. 4, pp. 682–688, 1999.

[13] B. L. Stevens, F. L. Lewis, and E. N. Johnson, *Aircraft Control and Simulation*. Wiley, 2016.

[14] F. J. Silvestre and G. Tissot, "Linear-quadratic, output-feedback flow control based on reduced order models." under consideration for publication in Journal of Fluid Mechanics.